Acta Mechanica Slovaca **28 (3): 6 - 17,** September **2024**
https://doi.org/10.21496/ams.2024.023

Acta Mechanica Slovaca
ISSN 1335-2393
www.actamechanica.sk

Crankshaft Bearing Hydrodynamic Lubrication Study in an Internal Combustion Engine (under variable dynamic loading)

Abdelmadjid Said [1,*], Abdelhamid Bounif [1], Patrick Maspeyrot [2]

[1] Mechanical Engineering Laboratory, Faculty of Science and Technology, University of Ain Temouchent-Belhadj Bouchaib, BP 284, 46000, Algeria
[2] Solid Mechanics Laboratory, UMR CNRS 6610, University of Poitiers, France

Abstract: The engine crankshaft bearing is an important component and vulnerable part of engine. Its operating condition significantly influences the dynamic performance, efficiency and overall reliability of the engine. In modern engine design, the main objective is to improve power output while minimizing friction losses and reducing fuel consumption. This present work concerns the study of the behavior in dynamic mode of the big-end and small-end bearings of connecting rod in internal combustion engine, taking into account the rupture and reformation of the fluid film in the contact region in the inactive cavitation zone. The most important operating parameters for the finite length case are calculated and compared to those obtained in the case of a short bearing hypothesis for the two types of connecting rod bearings: big-end and small-end. Solving the hydrodynamic lubrication problem in transient mode is carried out using the Booker mobility method, which is a fast and precise method using a computer language implemented in FORTRAN.

Keywords: hydrodynamic bearing, crankshaft, method of mobility, big-end, small-end, combustion engine.

1. Introduction

The connecting rod bearing is an important frictional component in an engine. Its operational condition directly impacts the engine's economy, reliability, durability, and lifespan. Continuous advancements in research and related technologies have led to significant improvements in the design capabilities of engine connecting rod bearings (big-end and small-end journals).

Many studies have explored the lubrication of connecting rod bearings. For instance, Liu examined the transient tribodynamic performance of the crankshaft-main bearing system during engine start-up [1], while Zammit investigated the lubrication of crankshaft bearings during engine warm-up [2]. Researchers like Inui, Jia and Galera et al. [3-5] focused on the factors influencing crankshaft bearing lubrication, and Gu et al. [6] assessed the performance of textured crankshaft bearings throughout an engine cycle.

Further, Francisco, Lavie, and Zhang et al. [7-9] explored optimizing crankshaft bearing lubrication. Ozasa et al. [10] introduced a simplified method for estimating engine bearing lubrication. Tabrizi et al. [11] compared different simulation models for connecting rod bearings, and Toshihiro et al. [12] studied lubrication in gasoline engine connecting rod bearings.

Additionally, Bi and Chen et al. [13,14] investigated lubrication in turbocharged engine main bearings. Choi et al. [15] analyzed dynamically bearing elastohydrodynamic

*** Corresponding author:** Abdelmadjid Said, ***E-mail address:*** *abdelmadjid.said@univ-temouchent.edu.dz*

lubrication, accounting for multi-flexible-body dynamics. Shao et al. [16] examined the lubrication performance of the engine main bearing system, including the cylinder block and crankshaft connecting rod. Zhao et al. [17] analyzed lubrication performance under typical operating conditions for marine engine main bearings.

In the present study, we analyzed the behavior of a smooth bearing supplied with an axial groove under transitory load (variable load in time, in module and direction) by using hydrodynamic study and computing performance analysis. These types of bearing are met in the connecting rods (big-end and small-end journal) of the vehicle engines.

We are interested especially in the short bearing, where the report/ratio length to the diameter of the bearing (L/D) is weak and the circumferential gradient of pressure is neglected; but in this case, it would be interesting to compare the results found with those of a finite length bearing.

The modeling of the problem of hydrodynamic lubrication in transitory mode leads us, with a partial derivative equation, known as "Equation of Reynolds" [18], which governs the flow of the fluid in the contact, and with a geometrical equation which defines the geometry of this contact. The Reynolds equation is numerically integrated using finite difference methods (FDM) combined with an iterative method taking into account Reynolds boundary conditions [18].

Of all the methods suggested, that of Booker [19] associated with an iterative method, appears best adapted to this type of problem. A computer code was developed using the FORTRAN programming language, allowing the calculation of the most important parameters that characterize the operation of a bearing working in dynamic mode (trajectory of the center of the shaft in the bearing, minimum thickness of the lubricating film in the contact, friction torque, fluid leakage flow rate and pressure field).

Determining the minimum thickness of the fluid film separating two contacting surfaces makes it possible to assess the risks of seizure, particularly in small end journal. Also, the effect of a variation of the dynamic viscosity of lubricant on the characteristics of bearing is studied. In the context of a machine, particularly in an internal combustion engine, the terms "big end journal" and "connecting rod journal" refer to specific parts of the connecting rod, which is a critical component in converting linear motion into rotational motion.

1.1. Big-end Journal

The "big-end" of the connecting rod is the larger, thicker end, typically attached to the crankshaft. The journal at this end is called the "big-end journal", it plays a crucial role in connecting piston to the crankshaft and transmitting the linear motion of the piston to rotational motion of crankshaft.

1.2. Small-end Journal

The "small-end" of the connecting rod is the smaller, thinner end, usually attached to the piston. The journal at this end is known as the"small-end journal", it connects to the piston pin, allowing the piston to pivot and move within the cylinder.

The terminology "big-end" and "small-end" is commonly used due to the size and relative importance of these ends in the engine's operation. The "big-end journal" is usually more substantial and handles greater forces, while the "small-end journal" is relatively smaller and is responsible for connecting the piston to the connecting rod, like the Figure 1.

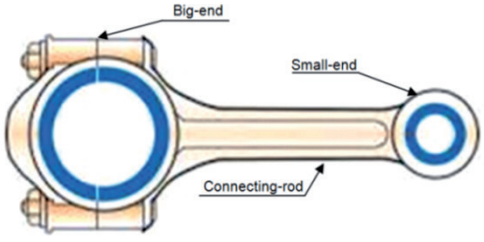

Figure 1: "Big-end" and "Small-end" journal.

2. Problem Formulation

The study of the hydrodynamic behavior of a contact lubricated by a Newtonian fluid consists in solving the hydrodynamic equation of viscous thin films (Reynolds equation) which is a second-order partial differential equation of elliptic type whose main unknown is the pressure. The value of the pressure in the film depends not only on the geometry of the contact and its kinematics, but also on the boundary conditions on the pressure retained at the time of resolution.

A hydrodynamic bearing is composed of two elements, the shaft of radius R_a, the bearing (bushing) of internal radius Rc and the length L, as shown in Figure 2.

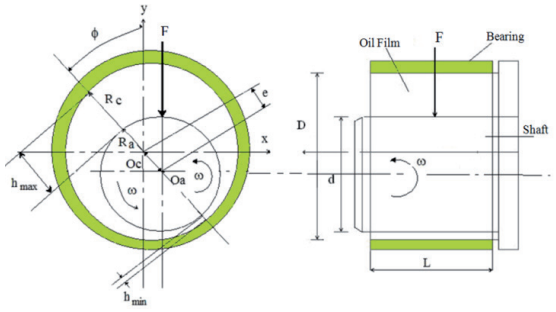

Figure 2: Sketch of hydrodynamic bearing.

2.1. Equation of Reynolds in transient mode

Reynolds equation translates the law of conservation of the flow in the contact. It is deduced from the Navier-Stokes equations [18], this equation is written:

$$\frac{\partial}{\partial\theta}\left(H^3\frac{\partial P}{\partial\theta}\right)+\left(\frac{R}{L}\right)^2\frac{\partial}{\partial Z}\left(H^3\frac{\partial P}{\partial Z}\right)=12\mu\frac{LD}{F\left(\frac{C}{R}\right)^2}\left[\left(\dot{\phi}-\varpi\right)\mu\sin\theta+\dot{\mu}\cos\theta\right] \quad (1)$$

With: $\theta = X/R$, $H = h/C$, $Z = z/L$, $P = p.(L.D/F)$

$\varpi=\left(\varpi_a+\varpi_c\right)/2-\dot{\psi}$

2.2. Boundary conditions of film

Solving equation (1) requires boundary conditions on the pressure. These conditions, called Reynolds boundary conditions, are generally used in the case of hydrodynamic bearings. By measuring atmospheric pressure as a reference, they are written:

Following O_z:

$$\bar{P}\left(\theta_s, Z=\pm 1/2, t\right)=0$$

Following θR:

$$\bar{P}\left(\theta_s=0, Z, t\right)=\bar{P}\left(\theta_s=2\pi, Z, t\right) \quad (2)$$

On the film frontier:

$$\bar{P}\left(\theta_s, Z, t\right)=0 \quad and \frac{\partial\bar{P}\left(\theta_s, Z, t\right)}{\partial\theta}=0$$

$$\bar{P}\left(\theta_s, Z, t\right)=0 \quad IF \quad \theta_s\langle\theta\langle 2\pi$$

Where: θ_s is the circumferential coordinate.

2.3. Geometrical Equation of Film

The geometrical relation between the thickness of fluid film H and the relative position of the journal which is defined by the eccentricity e at every moment is written:

$$h(\theta,t)=C\cdot\left(1+\varepsilon\cdot\cos\theta\right) \quad (3)$$

3. Resolution of the Problem

Among all the methods proposed for solving the problem of hydrodynamic lubrication of components operating in transient modes, the method presented by Booker [20] appears to be the most suitable.

3.1. Method of Mobility for Finite Length Bearing

The second member of the equation (1) revealed the two unknown factors of the problem $(\varepsilon \text{ and } \phi)$. In order to simplify Reynolds equation, Booker [20] proposed to express two velocities $(\dot{\varepsilon} \text{ and } \dot{\phi})$ according to the mobility components as in (4).

The solution is using an iterative method with two worth of $\dot{\varepsilon}$ and $\dot{\phi}$ until the load hydrodynamic $W(T)$ calculated either equal and opposed to the load applied $F(T)$. The two velocities $\dot{\varepsilon}$ and $\dot{\phi}$ according to the functions $M\varepsilon$ and $M\phi$ are expressed as follows:

$$\begin{cases}\dot{\varepsilon}=\dfrac{F\left(C/R\right)^2}{\mu LD}M_\varepsilon\\ \dot{\phi}=\dfrac{F\left(C/R\right)^2}{\mu LD\varepsilon}M_\phi+\varpi\end{cases} \quad (4)$$

These two functions defined as the components of a vector $\overrightarrow{M}$ called vector of mobility, can be written:

$$\begin{cases}M_\varepsilon=+M\cdot\cos\alpha\\ M_\phi=-M\cdot\sin\alpha\end{cases} \quad (5)$$

With: α angle between the mobility vector and the eccentricity direction, as shown in Figure 3 below:

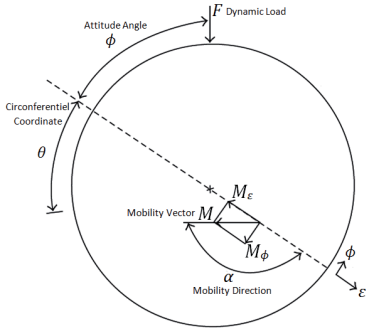

Figure 3: Designation of mobility vector.

By considering relations (4) and (5), and setting: $P=\overline{P}\cdot M$, then the modified Reynolds equation (1) takes the form:

$$\frac{\partial}{\partial\theta}\left(H^3\cdot\frac{\partial P}{\partial\theta}\right)+\left(\frac{R}{L}\right)^2\cdot\frac{\partial}{\partial Z}\left(H^3\cdot\frac{\partial P}{\partial Z}\right)=12\cdot\cos\left(\theta+\alpha\right) \quad (6)$$

It is noted that the second member of equation (6) uses only one unknown which is the direction of mobility α. The resolution of the pressure field in the lubricating film requires the calculation of the angle α which is given at each iteration using an iterative numerical interpolation method.

The components of the hydrodynamic load of the film are then determined and are written:

$$\bar{W}_{\varepsilon} = \int_{-1/2}^{+1/2}\int_{\theta_e}^{\theta_s} \bar{p}(\theta, Z)\cdot\cos\theta\cdot d\theta\cdot dZ$$
$$\bar{W}_{\phi} = \int_{-1/2}^{+1/2}\int_{\theta_e}^{\theta_s} \bar{p}(\theta, Z)\cdot\sin\theta\cdot d\theta\cdot dZ \qquad (7)$$

This allows us to calculate the modulus of the mobility vector and the attitude angle:

$$M = \frac{2}{\sqrt{\bar{W}_{\varepsilon}^2 + \bar{W}_{\varepsilon}^2}} \text{ and } \phi = Artg\left[\frac{\bar{W}_{\phi}}{\bar{W}_{\varepsilon}}\right] \qquad (8)$$

3.1.1. Determination of the operation parameters

3.1.1.1. Trajectory of the center of the shaft

The trajectory is obtained, for the step of time considered Δt, by integrating the speed of the center of the shaft at a given instant. The equation of motion in the calculation frame fixed at the bearing is written:

$$\frac{d\vec{\varepsilon}}{dt} = \frac{F\left(\frac{C}{R}\right)^2}{\mu L D}\vec{M} + \overrightarrow{\varpi \wedge \varepsilon} \qquad (9)$$

With: $\varpi = \frac{\varpi_a - \varpi_c}{2}$ average angular velocity of the journal and the bearing (bushing).

3.1.1.2. Minimal Film Thickness

For a perfectly aligned trajectory, the geometric equation between the thickness of the lubricating film H and the relative position with respect to the shaft which is defined by the eccentricity ε at each instant is:

$$h(\theta, t) = C\cdot(1 + \varepsilon\cdot\cos\theta)$$

So, for an angular position: $\theta = \pi$, she is written:

$$h_{min} = C\cdot(1 - \varepsilon) \qquad (10)$$

3.1.1.3. Friction Torque

The friction torque can be written as follows:

$$C = C_p + C_g^{\theta_e\cdot\theta_s} + C_{ina} \qquad (11)$$

The actual value of the friction torque takes into account the fact that the active zone $\left(C = C_p + C_g^{\theta_e\cdot\theta_s}\right)$, and which assumes the bearing is completely filled with fluid $\left(C = C_p + C_g^{0.2\pi}\right)$.

Where:

$$C_p = \int_{-L/2}^{+L/2}\int_{\theta_e}^{\theta_s} \frac{R}{2}\cdot\frac{\partial P}{\partial\theta}\cdot h\cdot d\theta\cdot dZ$$

due to pressure gradient

$$C_g^{\theta_e\cdot\theta_s} = \int_{-L/2}^{+L/2}\int_{\theta_e}^{\theta_s} R^2\cdot\frac{(U_a - U_c)}{h}\cdot\mu\cdot d\theta\cdot dZ \qquad (12)$$

due to sliding surfaces

$$C_{ina} = \int_{-L/2}^{+L/2}\int_{\theta_s}^{\theta_e+2\pi} R^2\cdot\frac{(U_a - U_c)}{h^2}\cdot h_s\cdot\mu\cdot d\theta\cdot dZ$$

in the inactive zone.

3.1.1.4. Bearing Leakage Flow

The bearing leakage rate is obtained by integrating the fluid velocity in the axial direction across the film section:

$$Q = -\frac{R}{6\cdot\mu}\cdot\int_0^{2\pi} h^3\cdot\frac{\partial P}{\partial Z}\cdot d\theta, \quad Z = L/2 \qquad (13)$$

3.2. Method of Mobility for Short Bearing

When the L/D ratio (length/diameter ratio) of the bearing is small, meaning less than 1/6, the circumferential pressure gradient can be neglected compared to the axial pressure gradient [18]. In the scenario where the bearing is subjected to dynamic loads and considering this assumption, the dimensionless Reynolds equation is expressed as follows:

$$\left(\frac{R}{L}\right)^2\frac{\partial}{\partial Z}\left(H^3\frac{\partial P}{\partial Z}\right) = 12\,M\cos(\theta + \alpha) \qquad (14)$$

The assumption of a short bearing does not allow the use of Reynolds boundary conditions. Therefore, the most satisfactory boundary conditions are those of Gümbel, which are:

$$\begin{cases} P(\theta, Z = -L/2) = P(\theta, Z = +L/2) = 0 \\ P(\theta, Z) \geq 0 \qquad \forall\ \theta \text{ and } Z \end{cases} \qquad (15)$$

Using these boundary conditions allows us to obtain the solution to equation (14), which gives:

$$P(\theta, Z) = 24\frac{\left(L/D\right)^2}{H^3}\left(Z^2 - \frac{1}{4}\right)M\cos(\theta + \alpha) \qquad (16)$$

Similar of the case of a bearing with finite length, the hydrodynamic load is, at every moment, equal and opposite of the applied load (equation (7)). From equations (7) and (16), a system of two equations is derived, written as:

$$\begin{cases} I_1 M_\phi + I_3 M_\varepsilon = \dfrac{\cos\phi}{2\left(\dfrac{L}{D}\right)^2} \\ I_2 M_\phi + I_1 M_\varepsilon = \dfrac{\sin\phi}{2\left(\dfrac{L}{D}\right)^2} \end{cases} \quad (17)$$

Where:

$$I_1 = \int_{\theta_e}^{\theta_s} \frac{\cos\theta \sin\theta}{(1+\varepsilon\cos\theta)^3} d\theta$$

$$I_2 = \int_{\theta_e}^{\theta_s} \frac{\sin^2\theta}{(1+\varepsilon\cos\theta)^3} d\theta \quad (18)$$

$$I_3 = \int_{\theta_e}^{\theta_s} \frac{\cos^2\theta}{(1+\varepsilon\cos\theta)^3} d\theta$$

These integrals are expressed analytically in [18], where θ_e and θ_s represent respectively the inlet and outlet limits of the film. In the case of the short bearing: $\theta_s = \theta_e + \pi$.

$$\begin{cases} I_1 = \dfrac{-2\,\varepsilon\,\cos^3\theta_e}{\left(1+\varepsilon^2\cos^2\theta_e\right)^2} \\ I_2 = \dfrac{1}{\left(1-\varepsilon^2\right)^2}\left[\dfrac{\varepsilon\sin\theta_e\left[3+\cos^2\theta_e\left(2-5\varepsilon^2\right)\right]}{\left(1-\varepsilon^2\cos^2\theta_e\right)^2} + \dfrac{2\varepsilon^2-1}{\sqrt{1-\varepsilon^2}} Arctg\left(\dfrac{-\sqrt{1-\varepsilon^2}}{\varepsilon\sin\theta_e}\right)\right] \\ I_3 = \dfrac{\varepsilon\sin\theta_e}{1-\varepsilon^2}\left[\dfrac{\left[1+\cos^2\theta_e\left(\varepsilon^2-2\right)\right]}{\left(1-\varepsilon^2\cos^2\theta_e\right)^2}\right] + \dfrac{1}{\left(1-\varepsilon^2\right)\sqrt{1-\varepsilon^2}} Arctg\left(\dfrac{-\sqrt{1-\varepsilon^2}}{\varepsilon\sin\theta_e}\right) \end{cases} \quad (19)$$

The solution to the system (17) provides the components of the mobility vector:

$$\begin{cases} M_\varepsilon = \dfrac{I_2\cos\varphi + I_1\sin\varphi}{2\left(I_3 I_2 - I_1^2\right)\left(\dfrac{L}{D}\right)^2} \\ M_\phi = \dfrac{-\left(I_1\cos\varphi + I_3\sin\varphi\right)}{2\left(I_3 I_2 - I_1^2\right)\left(\dfrac{L}{D}\right)^2} \end{cases} \quad (20)$$

Determination of the mobility vector for a given operating point requires knowledge of the limits of the integration domain θ_e and θ_s, which can only be determined using an iterative solution method.

The trajectory of the shaft center inside the bearing and the minimum lubricant film thickness are obtained in the same way as in the case of a finite length bearing.

3.2.1. Friction Torque

Considering the hypothesis of a short bearing, the friction torque on the shaft and the bearing is due only to the sliding speed of the surfaces, so this torques are equal. The expressions for the friction torques are as follows:

– *Taking into account only the active zone:*

$$Ca = Cc = \frac{R^3 L\mu}{C}\frac{2\left(\omega_a - \omega_c\right)}{\sqrt{1-\varepsilon^2}}\left[Arctg\left(\sqrt{\frac{1-\varepsilon}{1+\varepsilon}}tg\frac{\theta}{2}\right)\right]_{\theta e}^{\theta s} \quad (21)$$

Where: $\theta_s = \theta_e + \pi$

– *Assuming the bearing is solid (Full):*

$$Ca = Cc = \frac{R^3 L\mu}{C}\left(\omega_a - \omega_c\right)\frac{2\pi}{\sqrt{1-\varepsilon^2}} \quad (22)$$

3.2.2. Bearing Leakage Flow

The axial leakage flow is given by:

$$Q = -\frac{R}{6\mu}\int_{\theta_e}^{\theta_s} h^3 \left.\frac{\partial P}{\partial z}\right|_{z=L/2} d\theta \quad (23)$$

With: $\left.\dfrac{\partial P}{\partial z}\right|_{z=L/2} = 24\dfrac{\left(L/D\right)^2 C^3 F}{h^3 L^2 D} M\cos\left(\theta+\alpha\right)$

We found:

$$Q = -2\frac{C^3 F}{\mu D^3} M\left[\sin\left(\theta_s+\alpha\right) - \sin\left(\theta_e+\alpha\right)\right] \quad (24)$$

Using Gümbel's boundary conditions allows us to write:

$$Q = 4\frac{C^3 F M}{\mu D^3} \quad (25)$$

4. Solving Algorithm

The Calculations were performed for both a finite-length bearing and a short bearing. In the case of the short bearing, the equation of Reynolds was simplified by assuming $\partial P / \partial\theta = 0$, which facilitated an analytical integration. These calculations were carried out at different times $(T = t + \Delta t)$ using the dynamic load data $F(T)$. To determine the pressure field within the fluid film, the finite difference method was applied to the Reynolds equation.

The resulting system of linear equations was then solved using the iterative Gauss-Seidel method with an over-relaxation coefficient. The integration of the pressure field obtained allowed to calculate the load supported by the bearing $W(T)$ as well as its orientation ϕ for a given direction of mobility ε.

Finally, the operational parameters were determined on the basis of these results using a program implemented in FORTRAN, as illustrated in the Flowchart below.

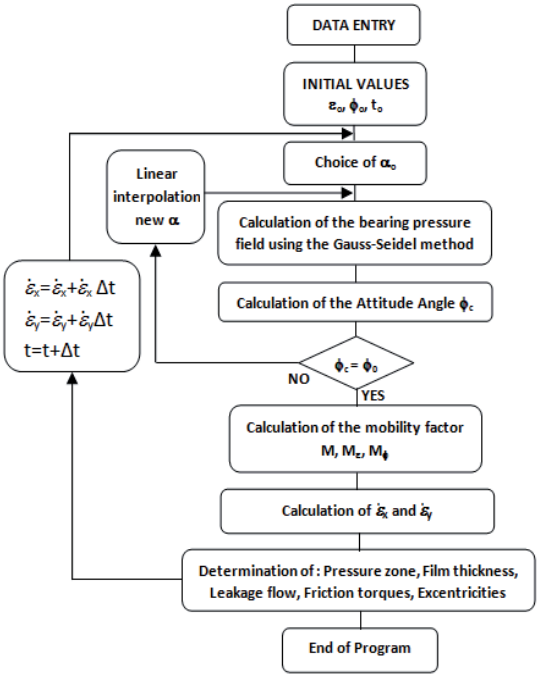

Figure 4: Solver Flow chart.

5. Numerical Results

The results obtained by applying the finite length bearing assumption are compared with those obtained by applying the short bearing simplification (neglecting the $\partial P / \partial \theta$ member) for both connecting rod bearings (Big-end and Small-end). The example used in this study is the crankshaft connecting rod bearing system of a four-cylinder Mitsubishi gasoline engine, which was previously studied by Huruma and Furuhama [21]. Engine parameters are detailed in Table 1. The load diagram applied to the big end journal is shown in Figure 5. The load diagram applied to the small end journal is calculated from the load diagram of the big end journal. We assumed that the mass of the connecting rod is 1 kg and positioned at the center of inertia G at 2/3 of its length from the piston axis O_3 as shown below:

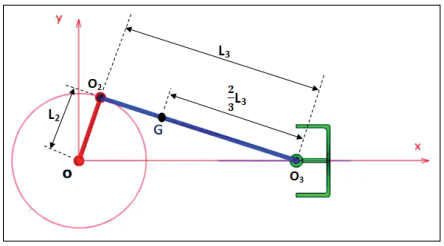

Figure 5: Geometry of the System.

Table. 1: Mitsubishi Four-cylinder engine parameter values

Parameters	Units	Big-end journal	Small-end journal
Length of the bearing : L	mm	25	23
Diameter of the bearing : D	mm	60	23
Radial clearence of the bearing : C	mm	0.036	0.015
Length / Diameter ratio of the bearing : L/D		0.42	1
(Boring x Travel) of the piston	mm	35 x 66	35 x 66
Distance between centres of rod : L_3	mm	119	119
Crankshaft radius : L_2	mm	33	33
Dynamic viscosity of the lubricant at 40°C : μ	Pa.s	0.0367	0.0367
Number of revolutions of the engine : ω_V	Tr/min	4000	4000
Meshing of Lubricant film : (N_θ x N_Z)	points	71 x 31	71 x 31

5.1. Big-end journal results

Using the load diagram (Figure 6) as input data, the results (Figures 7, 8, 9 and 10) obtained for the finite length bearing assumption are consistent with those obtained by applying the simplifying short bearing assumption, whose bearing length to diameter ratio is L/D = 0.42.

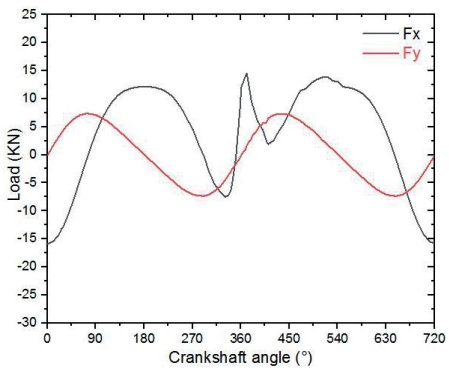

Figure 6: Load diagram (Big-end journal).

– The trajectories of the center of shaft within the bearing (figure 7) exhibit the same pattern and are closely aligned in both scenarios.
– As the assumption of a short bearing involves neglecting the circumferential pressure gradient $(\partial P / \partial \theta)$, the minimal lubricating film thickness (figure 8) obtained for the short bearing is slightly greater than that of the finite-length. This difference therefore results a higher pressure for the short bearing case.

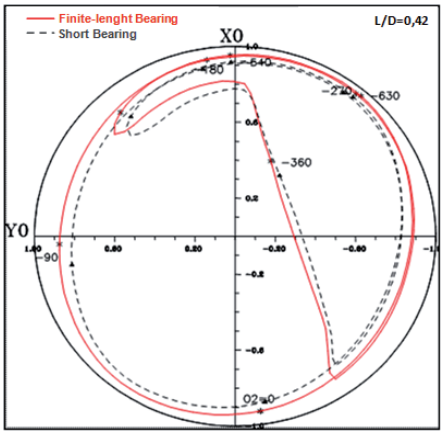

Figure 7: Trajectory of the center of shaft.

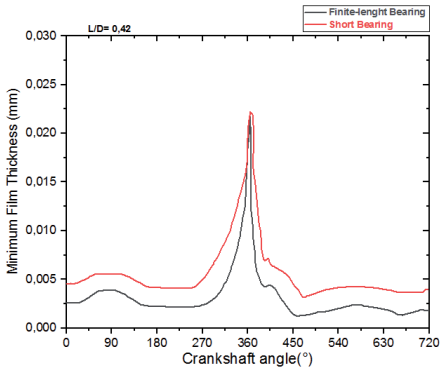

Figure 8: Variation of the minimum film thickness with the crankshaft angle.

– *The frictional torque (figure 9) for the short bearing is lower than that for the finite-length (Cc: Bush - Ca: shaft); this is primarily attributed to the increased film thickness and the omission of the circumferential pressure gradient in the case of the short bearing.*

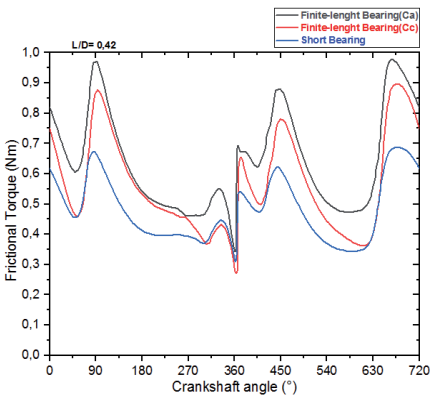

Figure 9: Variation of Frictional Torque with the crankshaft angle (full bearing).

– *The curves of the leakage flow (figure 10) for the short bearing hypothesis and that of finite-length are very close. This proximity in highlights the relationship between clearance, pressure and flow rate and describe that this two hypothesis are identical for our study.*

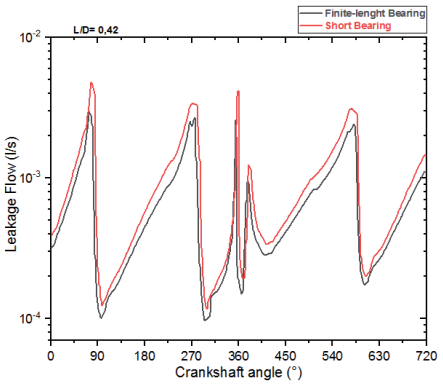

Figure 10: Leakage Flow with the crankshaft angle.

Understanding and managing leakage flow is essential for ensuring smooth operation, minimizing friction, and prolonging the lifespan of big-end journal of a connecting rod.

5.2. Small-end journal results

A notable distinction is observed between the load diagram applied to the big end journal (figure 6) and that applied to the small-end bearing (figure 11), primarily due to the effects of inertia. Taking into account the inertia of the connecting rod makes it possible to calculate the efforts of small-end. The load diagram (figure 11) applied to the small-end journal (F_s) is calculated from the load diagram (figure 6) applied to the big-end journal (F_b) by using this kinematic equation:

$$\begin{cases} F_b\vec{X}_0 + F_s\vec{X}_0 = m\dfrac{d^2X_G}{dt^2}\vec{X}_0 \\ F_b\vec{Y}_0 + F_s\vec{Y}_0 = m\dfrac{d^2Y_G}{dt^2}\vec{Y}_0 \end{cases}$$

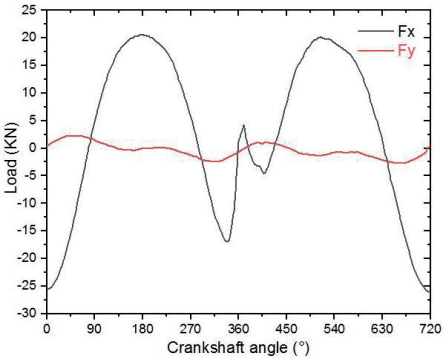

Figure 11: Load diagram (Small-end journal).

The trajectory of the center of the shaft within the bearing (Figure 12) demonstrates that the motion is particularly focused along the axis of the rod.

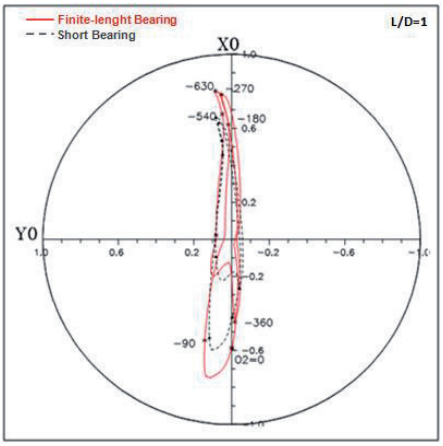

Figure 12: Trajectory of the center of shaft.

Minimal film thickness (Figure 13), frictional torques (on the shaft, bearing, and journal) (Figure 14), and leakage flow (Figure 15) exhibit very low values in three distinct zones as illustrated in the figures.

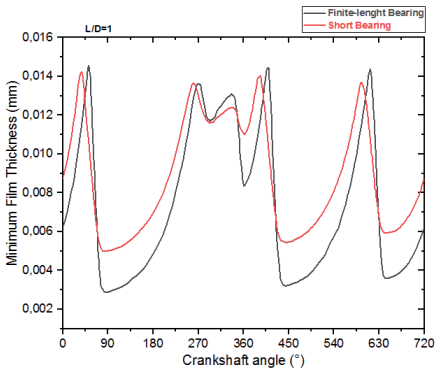

Figure 13: Variation of the Minimum Film thickness with the crankshaft angle.

The area where the lubricating film is very weak is when the average rotation speed of the bearing is zero. This description is satisfied by this equation: $\omega = 1/2 \cdot \omega_v \cdot (L_2 / L_3) \cdot \cos(\theta_v)$.

These zones (angles) correspond to three critical positions of the crankshaft shaft within the small end bearing by a loading cycle, which are: θ_v = 90°, 450° and 630°.

The bearing pressure at the lubricated contact level is generated by two effects: the first is due to pressure gradients, and the second is caused by the rotational motion of the two contacting surfaces. When the rotational speed of crankshaft is zero, the bearing pressure is solely attributed to the effect of pressure gradients, resulting in a reduction of the lubricating film thickness and the risk of film rupture, which could lead to contact between the two surfaces (risk of cavitation). Since the axial flow is highly dependent on the lubricating film thickness and the frictional torque, these two parameters have lower values in these three critical zones.

The frictional torque and axial flow are significantly lower compared to those calculated for the big-end journals.

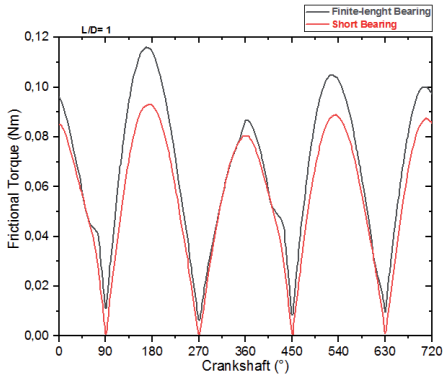

Figure 14: Variation of Frictional Torque with the crankshaft angle (full bearing).

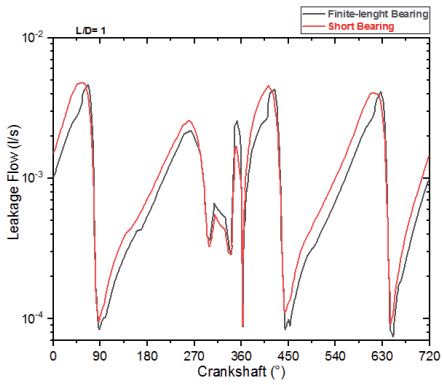

Figure 15: Leakage Flow with the crankshaft angle.

The difference between the curves obtained using the short bearing hypothesis and those obtained using the finite length bearing hypothesis is very close, which implies that this simplification is correct. It should be noted that using the short bearing hypothesis with the mobility method

significantly reduces the computational time required compared to using the finite-length bearing theory.

5.3. Influence of viscosity variation on Big-end journal characteristics

The dynamic viscosity of the lubricating film varied between 0.001 and 0.040 Pa.s for a big end journal. In this range of viscosities, it was observed that over a complete lubrication cycle, as the viscosity increased there was an increase in the minimum thickness of the lubricating film (Figure16), and a reduction in leakage flow (Figure17), and also an increase in friction torques (Figure18).

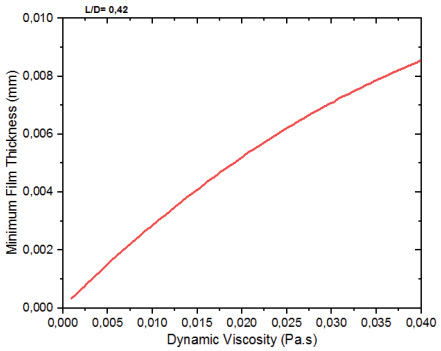

Figure 16: Variation of Minimum Film thickness with dynamic viscosity.

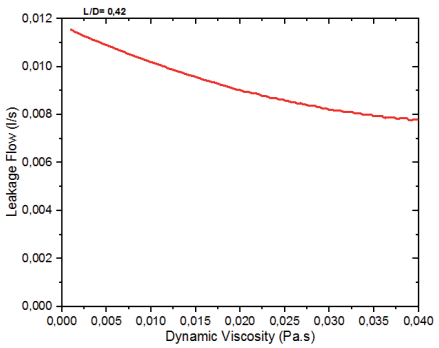

Figure 17: Variation of Leakage Flow with dynamic viscosity.

Based on these observations, the choice of oil significantly influences the performance of the lubricated contact. In fact, an inadequate choice of lubricant that leads to a reduction in the minimum film thickness can substantially increase the risk of seizures and damage through the rupture of the lubricating fluid film in the contact.

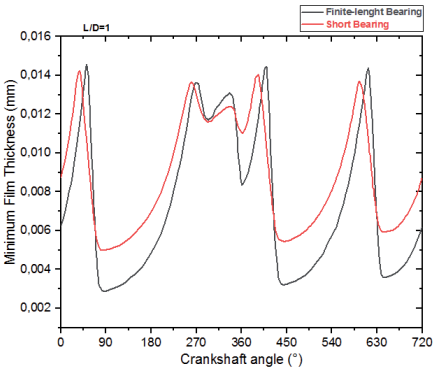

Figure 18: Variation of Frictional Torque with dynamic viscosity.

5.4 Hydrodynamic Pressure Calculation

In transient condition, the hydrodynamic pressure inside the bearing may exhibit considerable variation in response to rapid changes in shaft rotational speed and dynamic loads. This pressure fluctuation can have a significant influence on the bearing performance.

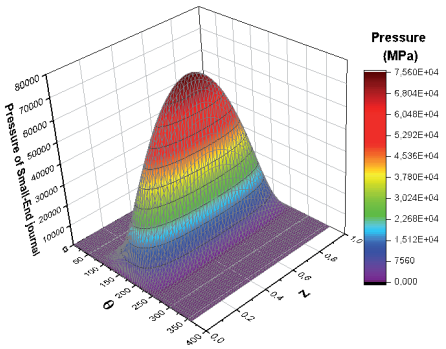

Figure 19: Variation of Hydrodynamic Pressure with θ and Z for Small-end journal.

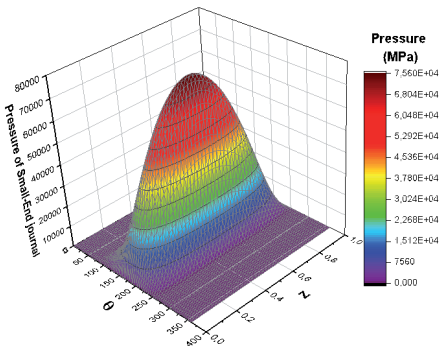

Figure 20: Variation of Hydrodynamic Pressure with θ and Z for Big-end journal.

Figures 19 and 20 describe the variation of pressure field for the short bearing hypothesis, and show areas of cavitation (P = 0) which means the rupture of the fluid film and the damage in the surface of the bearing, this area corresponds to:
$\theta \in [0;82]$ and $\theta \in [257;360]$.

For this coordinate (θ = 180°; z = 0.5), the fluid pressure reached its maximum in the case of the small-end with ($P_{max}=7,56.10^4$ MPa) and for that of the big-end with ($P_{max}=2,67.10^4$ MPa).

When the rotational speed of the shaft increases suddenly, the hydrodynamic pressure may temporarily decrease, which may cause momentary contact between the friction surfaces. This can lead to increased friction and wear in the bearing. Conversely, when the rotational speed suddenly decreases, the hydrodynamic pressure may increase temporarily, which can cause a momentary overload of the bearing.

6. Validation of Results

The results of our calculations show a remarkable alignment with the trends and behaviors observed in previous research and simulations carried out by Bonneau D [22] which concern the big end journal of a gasoline engine. This convergence reinforces the validity of our approach and confirms the robustness of our model.

Figure 21 shows a remarkable similarity with the results reported by our study because the curves of minimum fluid film thickness for our study and that of Bonneau D [22] have almost the same appearance, and reach their maximum at the crankshaft angle of 360°.

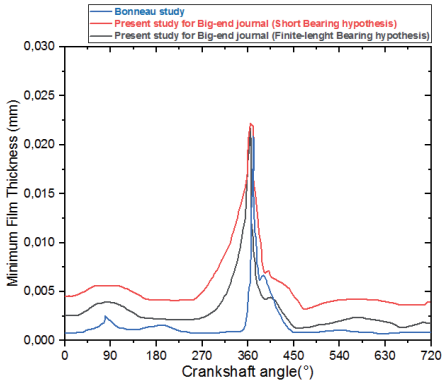

Figure 21: Variation of Minimum Film thickness with crankshaft angle for Present and Bonneau study.

Good agreement between a model and experiment cannot be considered as a verification of the validity of the approximate model results. Instead, such good agreement between model and experiment should be regarded as a verification of the utility of the model for prediction under the same conditions as used in the experiment.

7. Analysis of Computing Performances

Table 2 summarizes the comparison of averaged CPU Time Usage in second (s), RAM requirements in Megabytes (Mb), iterations count and precisions (%) with respect to the experiments for short bearing (SB) and Finite-length bearing (FB) models with (71 x 31 and 100 x 100) mesh numbers.

Table. 2: Comparison of averaged CPU Time Usage, RAM requirements, Iterations and Precisions for SB and FB with different mesh numbers

Model	*Short Bearing (SB)*	*Finite-lenght Bearing (FB)*
71 x 31 Mesh		
CPU (s)	727	1019
RAM (Mb)	40	51
Iteration Count	32	28
Precision (%)	-10% ±10	-3% ±3
100 x 100 Mesh		
CPU (s)	955	1391
RAM (Mb)	45	53
Iteration Count	51	32
Precision (%)	-5% ±5	-1% ±1

Increase in the mesh number method improves largely the precision of the results to the detriment of the RAM and the CPU performances. However, the two models cure these two disadvantages. Indeed, the approach allows an improvement in the precision and iteration count, definitely better than those carried out by the SB exercise. Nevertheless, in the case of SB we see a slight increase in the computation time (CPU) compared to the FB model. The detailed implementation with The SB and FB calculation can be very difficult because the RAM becomes very significant exceeding our current data-processing possibilities.

8. Conclusion

A good agreement is observed in the computational results between using the short bearing assumption (where the circumferential

pressure gradient is neglected: $\partial P / \partial \theta = 0$) and the finite-length bearing assumption. The use of the short bearing assumption in calculations is justified for cases with low L/D ratios (typically L/D < 0.5). This is applicable to the big-end journals of internal combustion engines (in our study, L/D = 0.42). Furthermore, utilizing this assumption in conjunction with the mobility method in dynamics significantly reduces computational time and RAM compared to using the finite-length bearing theory.

The small end bearings are prone to seizure due to their exposure to substantial dynamic loads, therefore the determination of operational parameters, in particular the minimum lubricant film thickness, allows to assess the risk of contact damage due to film rupture.

In a bearing, the viscosity of the lubricant is a crucial parameter that can be manipulated to modify the operational characteristics of bearing and extend its lifespan.

The developed computer code and the obtained results hold significance in the industrial context as they enable the prediction and understanding of the behavior of lubricated bearings, which currently represent the best technological solution available.

These converging observations underscore the reliability of our methodology and instill confidence in the relevance of our conclusions in comparison to the previous works notably that of Bonneau D [22].

References

[1] R C Liu, X H Meng, P Li. Transient tribodynamic analysis of crankshaft main bearing system during engines starting up. Proc IMechE Part J: J Engineering Tribology, 2018, 232(5): 535-549.

[2] J P Zammit, P J Shayler, R Gardiner. Investigating the potential to reduce crankshaft main bearing friction during engine warm-up by raising oil feed temperature. SAE Paper 2012-01-1216, 2012.

[3] M Inui, M Kobayashi, K Oowaki, et al. Analysis of oil film generation on the main journal bearing using a thin-film sensor and elasto-hydrodynamic lubrication (EHL) model. SAE Paper 2013-01-1217, 2013.

[4] D Jia, L Shen, Y Bi, et al. A study on the factors affecting the lubrication characteristics of connecting rod big-end bearing in diesel engine. Automotive Engineering, 2012, 34(11): 981-983.

[5] L Galera, A S Rodrigues. Optimization of lemon shape big end profile connecting rod under engine operation in elastohydrodynamic regime. SAE Paper 2014-36-0309, 2014.

[6] C X Gu, X H Meng, D Zhang, et al. A transient analysis of the textured journal bearing considering micro and macro cavitation during an engine cycle. Proc IMechE Part J: J Engineering Tribology, 2017, 231(10): 1289-1306.

[7] A Francisco, T Lavie, A Fatu, et al. Metamodel-assisted optimization of connecting rod big-end bearings. Journal of Tribology, 2013, 135: 0417041- 04170410.

[8] T Lavie, A Fransisco, A Fatu, et al. Multiobjective optimization of conrod big-end bearing lubrication using an evolutionary algorithm. Tribology Transactions, 2015, 58: 490-499.

[9] J H Zhang, G C Zhang, Z P He, et al. Optimization of crankshaft-bearing lubricating characteristics based on orthogonal experiment and neural network. Transactions of CSICE, 2011, 29(5): 461-467.

[10] T Ozasa, K Maitani, Y Fujimoto, et al. Simplified estimation method of bearing friction for engines. International J. of Engine Research, 2016, 17(8): 886-896.

[11] A A Tabrizi, A H Kakaei. Different simulation models of connecting rod hydrodynamic bearing. SAE Paper 2009-01-1863, 2009.

[12] O Toshihiro, N Masatoshi. Lubrication analysis of a con-rod bearing using a cycle simulation of gasoline engines with AF variation. SAE Paper 2011- 01-2118, 2011.

[13] Y Bi, Y Li, L Shen, et al. Lubrication property study of main bearing for turbocharged intercooled diesel engine. Chinese Internal Combustion Engine Engineering, 2012, 33(1): 87-92.

[14] X Chen, B Zu, Y Xu, et al. Influence of high-turbocharged on performance of main bearing in diesel engine. Chinese Internal Combustion Engine Engineering, 2015, 36(3): 6-11.

[15] J Choi, S S Kim, S S Rhim, et al. Numerical modeling of journal bearing considering both elastohydrodynamic lubrication and multi-flexible body dynamics. International Journal of Automotive Technology, 2012, 13(2): 255-261.

[16] K Shao, C W Liu, F R Bi, et al. Analysis of hydrodynamic loads on performance characteristics of engine main bearings. Proc IMechE Part J: Journal of Engineering Tribology, 2015, 229(6): 667-676.

[17] X Zhao, A Huang, Z Hu, et al. Analysis of main bearing lubrication performance of high-power marine diesel engine under typical operating conditions. Chinese Internal Combustion Engine Engineering, 2015, 36(5): 128-133.

[18] Frene J., Nicola D., Degueurce B., Berthe D., Godet M., Lubrification Hydrodynamique -Paliers et Butées, Editions Eyrolles, 1990, pp.253-286.

[19] Booker J.F., Dynamically Loaded Journal Bearings: Mobility Method of Solution. Journal of Basic Engineering, Trans. ASME, Série D, sept 1965, pp.537-546. http://dx.doi.org/10.1115/1.3650602.

[20] Booker J.F., Dynamically Loaded Journal Bearings: Numerical application of mobility Method. JOLT-ASME, Série F, January 1971, pp.168-176.

[21] Huruma M., Furuhama S., Measurement of the journal lows in con-rod Big-end bearing of automobile gasoline engine. Journal of Lubrication Technology, Avril 1973.

[22] Bonneau D., Fatu A., Souchet D., Internal Combustion Engine Bearing Lubrication in Hydrodynamic Bearings, ISTE, London and John Wiley & Sons, New York, 2014. http://dx.doi.org/10.1002/9781119005025